The Journal of Chemical Physics

Observation of photoassociation spectroscopy of ultralong $37D_{5/2} + 6S_{1/2}$ Cs_2 Rydberg molecules

Cite as: J. Chem. Phys. **152**, 084302 (2020); https://doi.org/10.1063/1.5132993
Submitted: 22 October 2019 . Accepted: 05 February 2020 . Published Online: 24 February 2020

Suying Bai, Xiaoxuan Han, Jingxu Bai, Yuechun Jiao, Huihui Wang, Jianming Zhao, and Suotang Jia

The Journal of Chemical Physics ARTICLE scitation.org/journal/jcp

Observation of photoassociation spectroscopy of ultralong $37D_{5/2} + 6S_{1/2}$ Cs_2 Rydberg molecules

Cite as: J. Chem. Phys. 152, 084302 (2020); doi: 10.1063/1.5132993
Submitted: 22 October 2019 • Accepted: 5 February 2020 •
Published Online: 24 February 2020

Suying Bai,[1,2] Xiaoxuan Han,[1,2] Jingxu Bai,[1,2] Yuechun Jiao,[1,2] Huihui Wang,[1,2] Jianming Zhao,[1,2,a)] and Suotang Jia[1,2]

AFFILIATIONS

[1]State Key Laboratory of Quantum Optics and Quantum Optics Devices, Institute of Laser Spectroscopy, Shanxi University, Taiyuan 030006, China
[2]Collaborative Innovation Center of Extreme Optics, Shanxi University, Taiyuan 030006, China

[a)]**Author to whom correspondence should be addressed:** zhaojm@sxu.edu.cn

ABSTRACT

We present an experimental observation of $37D_{5/2} + 6S_{1/2}$ Cs_2 Rydberg-ground molecules by employing a two-photon photoassociation method. Two distinct Rydberg-ground molecular signals, deep and shallow bound molecules, are observed at the red detuning of atomic line. In theory, the model of scattering interaction between the Rydberg electron and ground-state atom is used to simulate the experiments. Two potential energy curves with energy minimum, deep pure triplet $^3\Sigma$ and shallow hyperfine-mixed singlet–triplet $^{1,3}\Sigma$ potentials, refer to the attained Rydberg-ground molecular signals, respectively. Calculations of the binding energy of triplet $^3\Sigma$ and mixed $^{1,3}\Sigma v = 0$ states are compared with the measurements. The agreement between the calculated and measured values of the binding energy yields zero-energy scattering lengths $a_s^T(0) = -19.2a_0$ and $a_s^S(0) = -1.3a_0$, respectively.

I. INTRODUCTION

Photoassociation (PA) spectroscopy of ultracold atoms is a valuable technique for investigation of atomic collisions and production of ultracold molecules, which was theoretically proposed in 1987.[1] Ultracold molecules have been produced by PA in homonuclear nonpolar alkali molecules[2–4] and polar heteronuclear molecules.[5–8] PA spectroscopy can (i) serve as a significant approach for preparing ultracold molecules at micro-Kelvin temperature and (ii) give rise to a new high-resolution molecular spectroscopic technique (PA technique). PA spectroscopy has been an ideal method for detecting long-range molecular states, which provides abundant information on molecular structures in the near dissociation region.[9] In addition, it has been used to precisely measure the s-wave scattering length[10] and fundamental physical constants.[11]

Recently, PA spectroscopy offers unprecedented opportunities for the control of large scale molecules involving highly excited states, such as the Rydberg–Rydberg macrodimer[12–16] and Rydberg-ground molecules.[17–30] These types of molecules possess large permanent electric dipole moments of up to a kilo-Debye.[17,24] It makes ultralong-range Rydberg molecules a candidate for the realization of certain strongly correlated many-body gases[31] and quantum information processing.[32] Experiments on Rydberg-ground molecules were first reported with Rb $nS_{1/2}$ (n = 35–37) states[19] and later with Rb $nP_{1/2,3/2}$[22] and $nD_{3/2,5/2}$[23,28] states and recently with Cs $nS_{1/2}$[21,24] and $nP_{3/2}$[30] Rydberg states.

In this work, we report experimental observations and analysis of two-photon photoassociation spectroscopy of cesium atoms at the near dissociation of the $37D_{5/2} + 6S_{1/2}$ Rydberg molecule. At red detuning of the atomic line, the PA spectrum shows two distinct molecular signals at −56.0 MHz and −22.6 MHz, which come from the Rydberg-ground $37D_{5/2} + 6S_{1/2}(F = 4)$ Cs_2 molecules bound by the pure triplet $^3\Sigma$ potential and mixed singlet–triplet $^{1,3}\Sigma$ potential, respectively. The Rydberg-ground

molecular potential and vibrational functions are calculated and compared with the measurements of the PA spectrum, and the good agreement yields an appropriate zero-energy scattering length.

II. EXPERIMENTS

The two-photon PA experiments are performed in a crossed optical dipole trap (CODT), which is loaded from a standard cesium magneto-optical trap (MOT). The atomic density of CODT is $\sim 3 \times 10^{11}$ cm^{-3} measured by shadow imaging, and the estimated temperature is $T \sim 100$ μK, as shown in Fig. 1(a). The stray electric field is compensated by applying the electric potential at three pairs of electrodes placed beside the MOT. The corresponding stray field is less than 50 mV/cm, which leads to the molecular signal shift of $\lesssim$0.5 MHz. The two-photon PA scheme consists of an 852 nm and a 510 nm laser beams that are overlapped in a counter propagating geometry inside the CODT. The first photon, 852 nm laser (Toptical DLpro) with Gaussian waist $\simeq$80 μm, couples the lower ground state transition $|6S_{1/2}, \mathrm{F} = 4\rangle \rightarrow |6P_{3/2}, F' = 5\rangle$. The second photon, 510 nm laser (Toptical SHG110) with Gaussian waist $\simeq$40 μm, drives the up transition $|6P_{3/2}, F' = 5\rangle \rightarrow |37D_{5/2}\rangle$. The 852 nm laser frequency is locked to the transition of $|6S_{1/2}, \mathrm{F} = 4\rangle \rightarrow |6P_{3/2}, F' = 5\rangle$ by using the polarization spectrum technique[33] and blue shifted from the intermediate level by 360 MHz using a double-pass acousto-optic modulator (AOM). The 510-nm frequency is scanned from the Rydberg atomic line to ~100 MHz red detuned side. The frequency scan of the 510-nm beam is realized by using another double-passed AOM. During the frequency scan, the 510 nm laser power is kept fixed by using a PID (proportional integral derivative) feedback loop that controls the RF power supplied to the 510-nm AOM. The frequency of the 510-nm excitation beam is stabilized at a high-finesse F-P cavity with the 15 000 finesse.

After switching off trapping and CODT beams [see Fig. 1(b)], we apply two-photon PA laser beams for exciting the cesium ground $6S_{1/2}(F = 4)$ atoms to the $37D_{5/2}$ Rydberg state. During the PA laser pulse, the repumping laser keeps on for allowing a majority of the cesium atoms at hyperfine (F = 4) levels of the $6S_{1/2}$ state. To observe Cs $37D_{5/2}$ Rydberg photoassociation spectra, we apply a 3-μs excitation pulse with the power of the 852-nm beam (80 μW) and the 510-nm beam (10 mW). Then, Rydberg atoms and molecules are ionized with a ramped electric field, and the resultant ions are accelerated and detected with a microchannel plate (MCP) detector.

We first experimentally investigate a PA spectrum near the $37D_{5/2}$ resonance line, e.g., the $37D_{5/2} + 6S_{1/2}(F = 4)$ asymptote. Two free ground state atoms are excited to a bound state by the PA laser, where one atom is excited to the excited state and the other one stays in the ground state. When an atom is excited to the Rydberg state, the ground atom and Rydberg state atom could bind to form the Rydberg-ground molecules, only with the two free atoms fulfilling the following requirements: (i) the distance between the free atoms matches the molecular bond length and (ii) a PA-laser detuning from the Rydberg resonant line matches the molecules binding energy. Then, these molecules can directly be attained in a PA spectrum, and the relative binding energy is measured by a difference between the excitation frequency of the molecule and Rydberg atomic line.

In Fig. 2, we present a photoassociation spectrum of cesium atoms prepared in the $6S_{1/2}(F = 4)$ hyperfine levels to long-range cesium Rydberg molecules correlated with $37D_{5/2}$ Rydberg states. The spectrum, centered at the atomic resonance, is averaged by 5 independent measurements. The error bars indicate the standard errors of five independent measurements. In addition to the

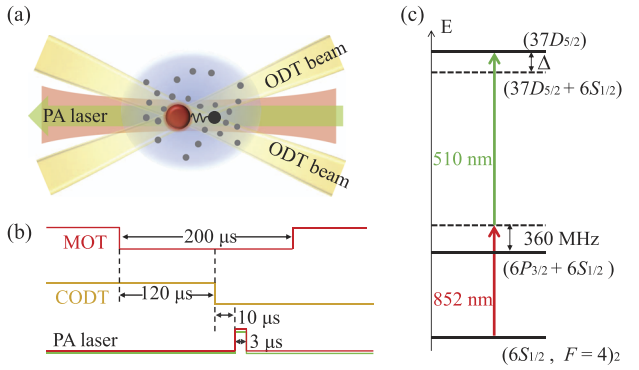

FIG. 1. (a) Experimental schematic of two-photon photoassociation spectra. Cesium atoms are trapped in a MOT (not shown here) and then loaded into a CODT. 852 nm and 510 nm lasers, overlapped in a counter propagating geometry inside the CODT, constitute a two-photon PA scheme. (b) Timing sequence. After switching off the trapping and CODT beams, the two-photon PA lasers are used to excite cesium ground atoms to form the Rydberg-ground molecules. A ramped electric field is finally applied to ionize the Rydberg atoms and molecules, and resultant ions are detected by using the microchannel plate. (c) Two-photon excitation diagram. The first photon, 852 nm laser, drives the $|6S_{1/2}, F = 4\rangle \rightarrow |6P_{3/2}, F' = 5\rangle$ transition, while the second photon, 510 nm laser, drives the $|6P_{3/2}, F' = 5\rangle \rightarrow |37D_{5/2}\rangle$ transition. The 852 nm laser frequency is blue shifted from $|6P_{3/2}, F' = 5\rangle$ by 360 MHz using a double-pass acousto-optic modulator (AOM). The 510-nm frequency is scanned to red detuning from the $37D_{5/2}$ Rydberg atomic line.

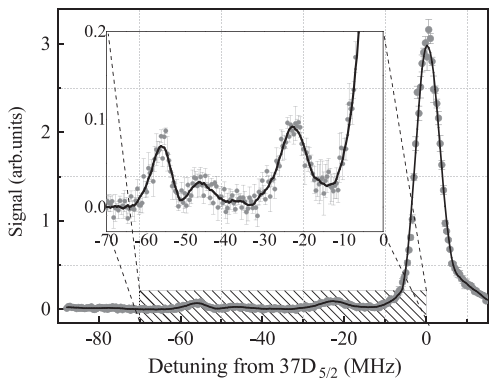

FIG. 2. Two-photon photoassociation spectra near the cesium $37D_{5/2}$ Rydberg state. The main peak at the 0-detuning position comes from the resonant excitation of the $37D_{5/2}$ atom, and two small peaks at detuning, −56.0 MHz and −22.6 MHz, are induced due to Rydberg-ground molecules, $37D_{5/2} + 6S_{1/2}(F = 4)$, denoted as the gray square. The Rydberg-ground molecular signal is obtained with respect to the pure triplet potential, $^3\Sigma$, and mixed singlet and triplet potential, $^{1,3}\Sigma$ (see the text for details). The inset is an enlargement of the gray region. Gray symbols and error bars show the original data; the black line displays smoothed average. The error bars are the standard errors of five independent measurements.

resonant excitation of the $37D_{5/2}$ Rydberg state at 0-detuning, a few photoassociation resonances at the red-detuned side are clearly shown in the shadowed region and enlarged in the inset of Fig. 2. The two strong photoassociation signals at −56.0 MHz and −22.6 MHz are clearly shown, which is attributed to the vibronic ground state of the pure triplet state $^3\Sigma$ ($v = 0$) and the hyperfine-mixed singlet–triplet state, $^{1,3}\Sigma$ ($v = 0$), respectively. The weak peak at about −45.5 MHz may come from the $^3\Sigma$ ($v = 1$) vibronic state.

III. THEORETICAL MODEL

To simulate the experimental data in Fig. 2, we calculate the molecular potential considering the pseudopotential due to the scattering interaction between the Rydberg electron and ground-state atom. In the theoretical model, the ground-state atom is considered as a point perturber. The total Hamiltonian[34] is written as

$$\hat{H}(\mathbf{r}, R) = \hat{H}_0 + \sum_{i=S,T} \hat{V}(\mathbf{r}, R)\hat{P}(i) + A_{HFS}\hat{\mathbf{S}}_2 \cdot \hat{\mathbf{I}}_2, \quad (1)$$

where $\hat{H}_0$ is the Hamiltonian of the unperturbed Rydberg atom including Rydberg quantum defects and the fine structure. The second term describes the scattering interaction between the Rydberg electron and ground atom, consisting of both spin-dependent singlet ($i = S$) and triplet ($i = T$) scattering channels, using the projection operators $\hat{P}(T) = \hat{\mathbf{S}}_1 \cdot \hat{\mathbf{S}}_2 + 3/4$ and $\hat{P}(S) = 1 - \hat{P}(T)$. The operators $\hat{\mathbf{S}}_1$ and $\hat{\mathbf{S}}_2$ are the electronic spins of the Rydberg and ground-state atoms, respectively. In the reference frame of the Rydberg ionic core, the scattering interaction is taken,[35]

$$\hat{V}(\mathbf{r}; R) = 2\pi a_s(k)\delta^3(\mathbf{r} - R\hat{\mathbf{z}}) + 6\pi[a_p(k)]^3\delta^3(\mathbf{r} - R\hat{\mathbf{z}})\overleftarrow{\nabla} \cdot \overrightarrow{\nabla}, \quad (2)$$

where $\mathbf{r}$ and $R\hat{\mathbf{z}}$ are the positions of the Rydberg electron and the ground-state atom, respectively. The $a_l(k)$ (l is the scattering partial-wave order, $l = 0$ for s-wave scattering, $l = 1$ for p-wave scattering, and so on) is the energy-dependent scattering length related to the scattering phase shifts $\eta_l(k)$ by $a_l(k)^{2l+1} = -\tan\eta_l(k)/k^{2l+1}$, and k is the electron momentum of the Rydberg atom. The scattering phase shifts $\eta_l(k)$ are extracted based on the approach of Ref. 36. In the non-relativistic approach, we use finite-range model potentials for the low-energy electron scattering, and related scattering lengths $a_s^S(k)$ and $a_s^T(k)$ are determined by numerically integrating the s-wave singlet and triplet scattering wave functions. The scattering momentum of the Rydberg electron is given by the quasiclassical expression, $k(r) = \sqrt{2E_{kin}} = \sqrt{2(E_{nl} + 1/r)}$ in atomic units, with the energy of Rydberg level $E_{nl} = -1/2(n - \delta_{nl})^2$ and δ_{nl} quantum defect of the Rydberg states. The last term in Eq. (1) demonstrates the hyperfine interaction of $\hat{\mathbf{S}}_2$ to the ground-state-atom nuclear spin $\hat{\mathbf{I}}_2$ with hyperfine parameter A_{HFS}.

Diagonalization of the Hamiltonian in Eq. (1) results in adiabatic potential curves $W_{ad}(R)$. Rovibrational states can be calculated with molecular Hamiltonian theory.[37–39] It is challenging for polyatomic molecules[40–43] to get accurate rovibrational energies. For the present diatomic molecule, accurate vibrational states $W_{ad,v}$ and corresponding wave functions $\Psi_{ad,v}(R)$ can be routinely obtained with potential $W_{ad}(R)$ and reduced mass 133 amu/2. In the calculation, we neglect the rotational motion of the molecule due to the narrow spacings between the accessible rotational levels compared to natural linewidths.

IV. RESULT AND DISCUSSION

In Fig. 3, we present the potential energy curves of the Rydberg molecule, asymptotically related to the $37D_{5/2}$ atomic line with and without considering the p-wave scattering interactions. At large internuclear separations, $R \gtrsim 2750a_0$, the scattering interactions between the Rydberg and perturber are negligible and the relative potential is nearly flat, corresponding to zero energy being the atomic asymptote of the isolated $37D_{5/2}$ Rydberg atom, which is the dissociation limit of the $37D_{5/2} + 6S_{1/2}(F = 4)$ Rydberg-ground molecule. At $R \simeq 2250a_0$, the potential curves display the outermost energy minimum that is dozens of megahertz deep, where the electron–atom interaction is modeled via the s-wave scattering interaction forming a trilobite-type Rydberg molecule. The deep-well potential is due to the pure triplet scattering interaction, and the shallow-well potential is due to hyperfine-mixed singlet and triplet scattering interaction (see below for details). At small internuclear separations, $R \lesssim 1800a_0$, the potential curve is modeled via p-wave scattering, which pushes the inner lobes deep forming a few GHz-deep potential wells that are used to bind butterfly-type Rydberg molecules.[17,44] The butterfly-type Rydberg molecule is beyond this work and will be investigated in future. Close inspection of the outmost well demonstrates that the p-wave scattering has a negligible impact on the outermost potential well. Aiming to attain more accurate results, we calculate the potential curves below by including the p-wave scattering.

The potential energy curves of Fig. 3 are calculated with $a_s^T(0) = -21.7a_0$ and $a_s^S(0) = -3.5a_0$[30] for the $37D_{5/2}$ asymptote. The last lobe at $R \sim 2250a_0$ creates the outermost and deepest potential minimum that could bind ground atoms and form Rydberg molecules.

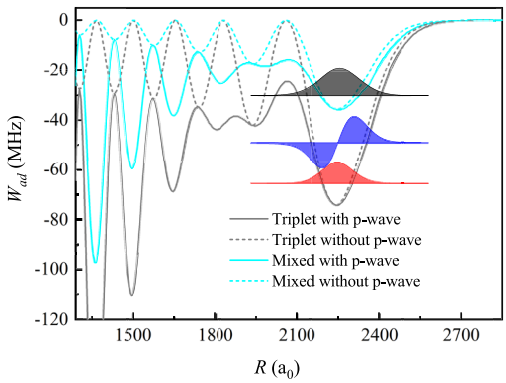

FIG. 3. Calculations of potential energy curves of the Rydberg-ground molecule that is asymptotically related to the $37D_{5/2}$ Rydberg atomic line with (solid) and without (dashed lines) taking the p-wave scatting interaction into account. The deep potential (gray) for the triplet $^3\Sigma$ state and shallow wells (blue) for hyperfine-mixed singlet–triplet potential $^{1,3}\Sigma$ states. The vibrational wave functions in the outermost wells are indicated in color filled curves for $v = 0$ and 1 of deep potential and $v = 0$ of shallow potential.

The depth of the outermost potential well is $V_{min} = -74.1$ MHz for the triplet potential. This supports two bound states corresponding to binding energies of −65.4 MHz ($v = 0$) and −49.1 MHz ($v = 1$), respectively. For the hyperfine-mixed potential curve, the outermost well has a minimum energy $V_{min} = -35.7$ MHz, which binds one vibrational state with a binding energy −30.3 MHz. It is noted that the calculated binding energy is ~14% larger than the measured binding energy, −56.0 MHz, for the $^3\Sigma$ ($v = 0$) vibrational state and ~25% larger than the measured energy, −22.6 MHz, for the $^{1,3}\Sigma$ ($v = 0$) state.

To attain agreement between measured and calculated values of the molecular binding energy, we tune the s-wave scattering-length functions $a_s^S(k)$ and $a_s^T(k)$ by phase shifting the wave function of the scattered electron at a small distance (0.1 a_0) from the scattering center. The phase shifts are parameterized by the zero-energy scattering lengths, $a_s^S(0)$ and $a_s^T(0)$. The zero-energy scattering length predicted by the theoretical calculation ranges from -21.7 to $-17a_0$ for $a_s^T(0)$ and from -1.33 to $-3.5a_0$ for $a_s^S(0)$.[44] We present the comparison of the measured binding energy of triplet $^3\Sigma(v = 0)$ [mixed $^{1,3}\Sigma(v = 0)$] to the calculations of a few $a_s^T(0)$ ($a_s^S(0)$) values in Table I (Table II).

The calculations indicate that the $^3\Sigma$ deep-well potential only depends on the triplet zero-energy scattering length $a_s^T(0)$, whereas the $^{1,3}\Sigma$ shallow-well potential depends on both $a_s^T(0)$ and $a_s^S(0)$. To fit our experimental observations, we first adjust triplet phase shifts and further the scattering length at step $0.1a_0$ and calculate the binding energy of the deep-well potential. The comparison with the experimental observation yields $a_s^T(0)$. The fitting procedure is similar to Ref. 28. In Table I, we present the calculated deep-well depth and corresponding binding energy of vibrational states $v = 0$ and $v = 1$ with fixed $a_s^S(0) = -1.0a_0$ and a different $a_s^T(0)$ value that is taken from Refs. 45 and 46. In the last line, we also display measured binding energies of the $^3\Sigma$ ($v = 0$ and 1) molecular state. It is found that the $a_s^T(0) = -19.2a_0$ yields a good reproduction of the $^3\Sigma(v = 0)$ molecular signal of the experimental observation. Then, we adjust singlet phase shifts to obtain the singlet $a_s^S(0)$ using a similar procedure mentioned above. In Table II, we present the calculated values of the shallow-well potential with $a_s^T(0) = -19.2a_0$ and different $a_s^S(0)$ and the measured binding energy in the last line. The comparison between the calculated and measured values of binding energies of the $^{1,3}\Sigma$ ($v = 0$) state yields a singlet scattering length of $a_s^S(0) = -1.3a_0$.

TABLE I. Comparison of measured and calculated values of the outermost deep-well depth and binding energy of $v = 0$ and $v = 1$ vibrational states in MHz relative to the dissociation limit of the $37D_{5/2} + 6S_{1/2}(F = 4)$ molecule for different $a_s^T(0)$ and fixed $a_s^S(0) = -1.0a_0$.

Theor.	Triplet potential		
$a_s^T(0)$	V_{min}	$V_{v=0}$	$V_{v=1}$
−21.7[a]	−74.1	−65.4	−49.1
−17[b]	−55.5	−48.3	−34.5
−18.7	−62.2	−54.4	−40.1
−19.2	−64.2	−56.2	−41.6
Expt.		−56.0 ± 0.2	−45.5 ± 0.4

[a]The $a_s^T(0)$ value in the first column is from Ref. 45.
[b]The $a_s^T(0)$ value in the first column is from Ref. 46.

TABLE II. Comparison of measured and calculated values of the outermost shallow-well potential and binding energy of vibrational state $v = 0$ in MHz relative to the dissociation limit of the $37D_{5/2} + 6S_{1/2}(F = 4)$ molecule for different $a_s^S(0)$ and fixed $a_s^T(0) = -19.2a_0$.

Theor.	Hyperfine-mixed potential	
$a_s^S(0)$	V_{min}	$V_{v=0}$
−3.5[a]	−31.3	−26.3
−2.4[b]	−29.1	−24.5
−1.3	−27.1	−22.7
−1	−26.3	−22.1
Expt.		−22.6 ± 0.2

[a]The value $a_s^S(0)$ in the first column is from Ref. 30.
[b]The value $a_s^S(0)$ in the first column is from Ref. 47.

In Fig. 4(a), we present the potential-energy curves related to the $37D_{5/2} + 6S_{1/2}F = 4$ asymptote, calculated with the zero-energy scattering length $a_s^T(0) = -19.2a_0$ and $a_s^S(0) = -1.3a_0$. For comparison, we also display the two-photon PA spectrum of the $37D_{5/2} + 6S_{1/2}(F = 4)$ Rydberg molecule in Fig. 4(b). The molecular signals of vibration level $v = 0$ are marked with triangles, showing a good agreement with the calculated results. The binding energies are measured as molecular line positions with respect to the $37D_{5/2}$ atomic line. Gaussian fittings to molecular peaks [blue lines in Fig. 4(b)] yield a binding energy of −56.0 ± 0.2 for the deep well triplet $^3\Sigma(v = 0)$ state and −22.6 ± 0.2 for the shallow well hyperfine-mixed singlet–triplet $^{1,3}\Sigma(v = 0)$ state. The errors represent Gaussian

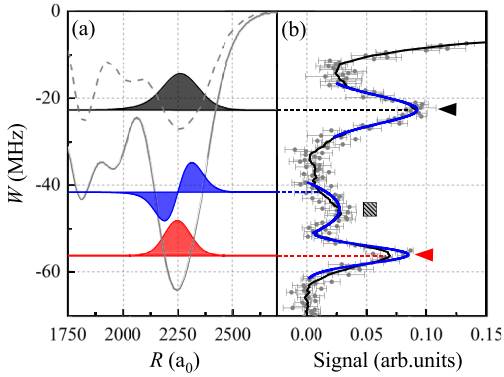

FIG. 4. Comparison between calculated potential energy curves and experimental measurement of two-photon PA spectra for the $37D_{5/2} + 6S_{1/2}(F = 4)$ Rydberg molecule. (a) Calculation of Rydberg-ground molecular potential curves (gray lines) and vibrational wave functions (colored lines). The shallow-well potential (dashed gray line) and deep-well potential (solid gray line) are induced by the hyperfine mixed singlet–triplet and pure triplet potentials, respectively. (b) Measurements of the two-photon PA spectra of the $37D_{5/2} + 6S_{1/2}(F = 4)$ Rydberg-ground molecule. The molecular signals for the vibration level $v = 0$ are marked with the triangles. The blue solid lines are Gaussian fittings to the molecular peaks.

TABLE III. Calculations of the binding energy of vibrational state $v = 0$ of $^3\Sigma$ and $^{1,3}\Sigma$ potential curves in MHz relative to the dissociation limit of $26P_{3/2}+6S_{1/2}(F = 3, 4)$ and $33P_{3/2}+6S_{1/2}(F = 3, 4)$ molecules.

	F = 4		F = 3	
n	$^3\Sigma$	$^{1,3}\Sigma$	$^3\Sigma$	$^{1,3}\Sigma$
26	−392.6	−126.4	−392.7	−189.6
33	−88.8	−32.0	−88.8	−45.5

fitting errors. The accuracy of the binding energy value is given by the laser linewidth and Gaussian fittings.

To corroborate our model, we further calculate the potential energy curves of $nP_{3/2} + 6S_{1/2}(F = 3, 4)$ Cs_2 molecules relative to $nP_{3/2}$ resonance atomic lines, investigated in Ref. 30. As an example, Table III demonstrates the calculated binding energy of triplet $^3\Sigma(v = 0)$ and hyperfine-mixed $^{1,3}\Sigma(v = 0)$ vibrational ground states of $26P_{3/2} + 6S_{1/2}(F = 3, 4)$ and $33P_{3/2}+6S_{1/2}(F = 3, 4)$ molecules. The calculations are in agreement with the experimental observation of Ref. 30 with discrepancy less than 2.5%.

V. SUMMARY

In summary, we have observed the two-photon photoassociation spectrum of the $37D_{5/2}$ Rydberg state and found two distinct peaks at the negative detuned position of the atomic line, which come from the Rydberg-ground molecules. We use the model of low-energy scattering interaction between the Rydberg electron and ground-state atom to simulate the experiment. We have compared the measured binding energy to the calculated one. It is found that the zero-energy scattering lengths $a_s^T(0) = -19.2a_0$ and $a_s^S(0) = -1.3a_0$ show good agreement with the experimental results for both triplet $^3\Sigma$ and hyperfine-mixed $^{1,3}\Sigma$ potential wells. The further calculations demonstrate that the extracted binding energy shows good agreement with the measurements for the large n range and different angular momenta of $nP_{3/2}$ in the literature.[30] In future work, we will investigate trilobite molecules for different nD_J Rydberg states and the properties such as vibrational wave function and dipole moments.

ACKNOWLEDGMENTS

We thank G. Raithel for valuable discussions on the calculation of the potential. This work was supported by the National Key R&D Program of China (Grant No. 2017YFA0304203), the National Natural Science Foundation of China (Grants Nos. 11434007, 61835007, 61675123, 61775124, and 11904215), Changjiang Scholars and Innovative Research Team in University of Ministry of Education of China (Grant No. IRT_17R70), and 1331 project.

REFERENCES

[1] H. R. Thorsheim, J. Weiner, and P. S. Julienne, Phys. Rev. Lett. **58**, 2420 (1987).
[2] J. M. Gerton, D. Strekalov, I. Prodan, and R. G. Hulet, Nature **408**, 692–695 (2000).
[3] U. Schlöder, T. Deuschle, C. Silber, and C. Zimmermann, Phys. Rev. A **68**, 051403(R) (2003).
[4] M. Viteau, A. Chotia, M. Allegrini, N. Bouloufa, O. Dulieu, D. Comparat, and P. Pillet, Science **321**, 232–234 (2008).
[5] J. Deiglmayr, A. Grochola, M. Repp, K. Mörtlbauer, C. Glück, J. Lange, O. Dulieu, R. Wester, and M. Weidemüller, Phys. Rev. Lett. **101**, 133004 (2008).
[6] S. Dutta, J. Lorenz, A. Altaf, D. S. Elliott, and Y. P. Chen, Phys. Rev. A **89**, 020702(R) (2014).
[7] D. Wang, J. Qi, M. F. Stone, O. Nikolayeva, H. Wang, B. Hattaway, S. D. Gensemer, P. L. Gould, E. E. Eyler, and W. C. Stwalley, Phys. Rev. Lett. **93**, 243005 (2004).
[8] A. J. Kerman, J. M. Sage, S. Sainis, T. Bergeman, and D. DeMille, Phys. Rev. Lett. **92**, 033004 (2004).
[9] W. Liu, R. Xu, J. Wu, J. Yang, S. S. Lukashov, V. B. Sovkov, X. Dai, J. Ma, L. Xiao, and S. Jia, J. Chem. Phys. **143**, 124307 (2015).
[10] J. Kim, S. Moal, M. Portier, J. Dugué, M. Leduc, and C. Cohen-Tannoudji, Europhys. Lett. **72**, 548 (2005).
[11] D. DeMille, S. Sainis, J. Sage, T. Bergeman, S. Kotochigova, and E. Tiesinga, Phys. Rev. Lett. **100**, 043202 (2008).
[12] C. Boisseau, I. Simbotin, and R. Côté, Phys. Rev. Lett. **88**, 133004 (2002).
[13] K. R. Overstreet, A. Schwettmann, J. Tallant, D. Booth, and J. P. Shaffer, Nat. Phys. **5**, 581 (2009).
[14] J. Deiglmayr, H. Saßmannshausen, P. Pillet, and F. J. Merkt, Phys. Rev. Lett. **113**, 193001 (2014).
[15] H. Saßmannshausen and J. Deiglmayr, Phys. Rev. Lett. **117**, 083401 (2016).
[16] X. X. Han, S. Y. Bai, Y. C. Jiao, L. P. Hao, Y. M. Xue, J. M. Zhao, S. T. Jia, and G. Raithel, Phys. Rev. A **97**, 031403(R) (2018).
[17] C. H. Greene, A. S. Dickinson, and H. R. Sadeghpour, Phys. Rev. Lett. **85**, 2458 (2000).
[18] I. Lesanovsky, P. Schmelcher, and H. R. Sadeghpour, J. Phys. B: At., Mol. Opt. Phys. **39**, L69 (2006).
[19] V. Bendkowsky, B. Butscher, J. Nipper, J. P. Shaffer, R. Löw, and T. Pfau, Nature **458**, 1005 (2009).
[20] V. Bendkowsky, B. Butscher, J. Nipper, J. B. Balewski, J. P. Shaffer, R. Löw, T. Pfau, W. Li, J. Stanojevic, T. Pohl, and J. M. Rost, Phys. Rev. Lett. **105**, 163201 (2010).
[21] J. Tallant, S. T. Rittenhouse, D. Booth, H. R. Sadeghpour, and J. P. Shaffer, Phys. Rev. Lett. **109**, 173202 (2012).
[22] M. A. Bellos, R. Carollo, J. Banerjee, E. E. Eyler, P. L. Gould, and W. C. Stwalley, Phys. Rev. Lett. **111**, 053001 (2013).
[23] D. A. Anderson, S. A. Miller, and G. Raithel, Phys. Rev. Lett. **112**, 163201 (2014).
[24] D. Booth, S. T. Rittenhouse, J. Yang, H. R. Sadeghpour, and J. P. Shaffer, Science **348**(6230), 99 (2015).
[25] T. Niederprüm, O. Thomas, T. Eichert, and H. Ott, Phys. Rev. Lett. **117**, 123002 (2016).
[26] T. Niederprüm, O. Thomas, T. Eichert, C. Lippe, J. PérezRíos, C. H. Greene, and H. Ott, Nat. Commun. **7**, 12820 (2016).
[27] K. S. Kleinbach, F. Meinert, F. Engel, W. J. Kwon, R. Löw, T. Pfau, and G. Raithel, Phys. Rev. Lett. **118**, 223001 (2017).
[28] J. L. Maclennan, Y. J. Chen, and G. Raithel, Phys. Rev. A **99**, 033407 (2019).
[29] A. T. Krupp, A. Gaj, J. B. Balewski, P. Ilzhöfer, S. Hofferberth, R. Löw, T. Pfau, M. Kurz, and P. Schmelcher, Phys. Rev. Lett. **112**, 143008 (2014).
[30] H. Saßmannshausen, F. Merkt, and J. Deiglmayr, Phys. Rev. Lett. **114**, 133201 (2015).
[31] H. Weimer, M. Müller, I. Lesanovsky, P. Zoller, and H. P. Büchler, Nat. Phys. **6**, 382–388 (2010).
[32] M. D. Lukin, M. Fleischhauer, R. Cote, L. M. Duan, D. Jaksch, J. I. Cirac, and P. Zoller, Phys. Rev. Lett. **87**, 037901 (2001).
[33] C. P. Pearman, C. S. Adams, S. G. Cox, P. F. Griffin, D. A. Smith, and I. G. Hughes, J. Phys. B: At., Mol. Opt. Phys. **35**, 5141 (2002).
[34] D. A. Anderson, S. A. Miller, and G. Raithel, Phys. Rev. A **90**, 062518 (2014).
[35] A. Omont, J. Phys. France **38**, 1343 (1977).

[36]A. A. Khuskivadze, M. I. Chibisov, and I. I. Fabrikant, Phys. Rev. A **66**, 042709 (2002).
[37]Y. G. Yang and O. Kühn, Mol. Phys. **106**, 2445–2457 (2008).
[38]Y. G. Yang and M. Meuwlya, J. Chem. Phys. **133**, 064503 (2010).
[39]Y. G. Yang, X. M. Liu, M. Meuwly, L. T. Xiao, and S. T. Jia, J. Phys. Chem. A **116**, 11134 (2012).
[40]Y. G. Yang and O. Kühn, Chem. Phys. Lett. **505**, 1–4 (2011).
[41]C. M. Liu, J. Manz, and Y. G. Yang, Phys. Chem. Chem. Phys. **18**, 5048–5055 (2016).
[42]Y. G. Yang, D. M. Jia, Y. J. Wang, H. J. Zhai, Y. Man, and S. D. Li, Nanoscale **9**, 1443 (2017).
[43]D. M. Jia, J. Manz, and Y. G. Yang, J. Phys. Chem. Lett. **10**, 4273–4277 (2019).
[44]M. T. Eiles, J. Phys. B: At. Mol. Phys. **52**, 113001 (2019).
[45]C. Bahrim, U. Thumm, and I. I. Fabrikant, J. Phys. B: At., Mol. Opt. Phys. **34**, L195 (2001).
[46]C. Bahrim and U. Thumm, Phys. Rev. A **61**, 022722 (2000).
[47]I. I. Fabrikant, J. Phys. B: At. Mol. Phys. **19**, 1527 (1986).